

# REACTION FORCE/TORQUE SENSING WHEEL SYSTEM FOR IN-SITU MONITORING ON LOOSE SOIL

Shoya Higa<sup>a</sup>, Kenji Nagaoka<sup>b</sup>, and Kazuya Yoshida<sup>c</sup>

<sup>a</sup> Tohoku University, [shoya@astro.mech.tohoku.ac.jp](mailto:shoya@astro.mech.tohoku.ac.jp)

<sup>b</sup> Tohoku University, [nagaoka@astro.mech.tohoku.ac.jp](mailto:nagaoka@astro.mech.tohoku.ac.jp)

<sup>c</sup> Tohoku University, [yoshida@astro.mech.tohoku.ac.jp](mailto:yoshida@astro.mech.tohoku.ac.jp)

---

## Abstract

Lunar/planetary exploration rovers are required to travel on loose soil. In such environments, wheel sinkage and slippage easily occur and adversely affect the mobility performance of the rovers. Therefore, we need to consider the wheel–soil interaction for appropriate mobility control. However, soil characteristics of the target environment of rovers are unknown and heterogeneous. Thus, unexpected wheel sinkage and slippage occur with rovers. It is expected that such phenomena can be avoided by appropriately estimating wheel conditions. Therefore, we proposed a sensing wheel system that estimates wheel sinkage/slippage and soil reaction force/torque. Previous work focused on an online estimation method of wheel sinkage/slippage using a time-of-flight (ToF) camera; through this method, online estimates of wheel sinkage/slippage could be made. In this study, we expand the previous system in order to develop a real-time sensing function of soil reaction force/torque. The proposed system can measure the reaction forces/torques by fixing a 6-axis force/torque (F/T) sensor onto the wheel axis. Traction tests were performed under several wheel configurations and traction load conditions to validate the projected wheel forces/torques. Experimental results showed that the sensing wheel precisely measured the drawbar pull, normal force, and wheel torque in real time.

**Keywords:** lunar/planetary rover, sensing wheel system, reaction force/torque

---

## 1. Introduction

Lunar/planetary exploration missions have been performed using unmanned mobile robots (rovers). Rovers allow for the direct investigation on the surface of a target celestial body and provide considerable scientific returns. Therefore, rovers will play a significant role in future lunar/planetary exploration missions. A major challenge is that the target environments of rovers are covered with fine granular regolith, where gravel and rocks are also widespread. Despite these environmental challenges, wheeled rovers have been utilized owing to their efficient mobility performance and high mechanical reliability. However, the rover struggles to follow the desired route because the rover traverses with wheel slippage and sinkage when it travels on deformable terrains, such as loose soil. Once the rover encounters increasing wheel sinkage and slippage, it becomes exceptionally difficult to reduce these wheel sinkage and slippage conditions. Therefore, rover operators have avoided steep-sloped, sandy terrains whenever possible. However, the most interesting areas for scientists are generally in challenging environments, such as on the rims and inside of craters. In order to explore such challenging targets, early detection of increases in wheel sinkage and slippage is essential. Large wheel sinkage and slippage are induced by a limitation of the conventional wheel–soil interaction model, unknown terrain characteristics, and other unpredictable factors. Therefore, to prevent lunar/planetary rovers from lapsing into a

---

The authors are solely responsible for the content of this technical presentation. The technical presentation does not necessarily reflect the official position of the International Society for Terrain Vehicle Systems (ISTVS), and its printing and distribution does not constitute an endorsement of views which may be expressed. Technical presentations are not subject to the formal peer review process by ISTVS editorial committees; therefore, they are not to be presented as refereed publications. Citation of this work should state that it is from an ISTVS meeting paper. EXAMPLE: Author's Last Name, Initials. 2014. Title of Presentation. The 19th International & 14th European-African Regional ISTVS Conference, Budapest, Hungary. For information about securing permission to reprint or reproduce a technical presentation, please contact ISTVS at 603-646-4405 (72 Lyme Road, Hanover, NH 03755-1290 USA)

---

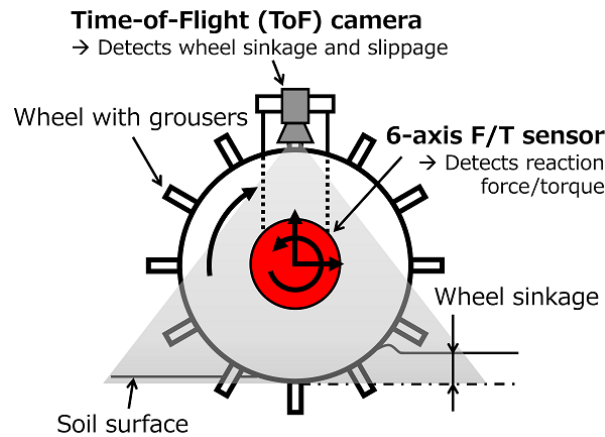


*Fig. 1 Conceptual diagram of a wheel system for wheel performance estimation.*

serious-slip condition, the current wheel–soil interaction model must be reconsidered, and the terrain characteristics of the target environments should be re-evaluated in situ.

To precisely clarify the wheel–soil interaction, we measured the stress distribution of a wheel with and without grousers (Higa et al., 2016b, 2015). These experimental results are significant achievements for remodeling the conventional theory using flat and homogeneous soil conditions; however, real terrain conditions include rough and heterogeneous soil, and thus, there is uncertainty in the mobility prediction of the rover. Typical rovers can obtain wheel torque and environmental information using optical cameras. Wheel torque can be estimated by the motor current of the wheel, and optical cameras can be used to estimate wheel conditions. The exploration targets of future rovers will include more challenging areas than past and ongoing missions. To travel safely on deformable terrain with wheeled vehicles, estimating each wheel performance online is important. Therefore, in this study, we have proposed a system for online wheel performance estimation.

There have been several related studies that estimated wheel performance (wheel sinkage/slippage and forces/torques acting on a wheel). Iagnemma et al. addressed the online estimation of terrain parameters by identifying the force acting on the wheel in the conventional model (Iagnemma et al., 2004). This study was accomplished by sensing the torque and reaction forces applied to a mobile robot by the terrain. Terrain forces and parameter estimates were also conducted by using classical wheel–soil interaction models (Ray, 2009). Nagatani et al. estimated the drawbar pull accurately by directly measuring the normal stress distribution beneath a wheel using pressure sensor arrays attached to the wheel surface (Nagatani et al., 2009). Estimations of wheel sinkage have been performed by determining the wheel contact angle (Shirai and Ishigami, 2014). Iizuka et al. proposed a sensing wheel that directly detects wheel sinkage using strain gages (Iizuka et al., 2014a, 2014b). Nagatani et al. studied a visual odometry system using a telecentric camera on loose soil (Nagatani et al., 2010). Estimations of wheel sinkage/slippage based on images of the side surface of the traveling wheel have also been studied (Hegde et al., 2013; Milella et al., 2006; Reina et al., 2006). Wheel slippage detection has been performed by measuring the wheel motor current (Ojeda et al., 2006). These related works only addressed estimations of either the wheel sinkage/slippage or the reaction force acting on the wheel based on the conventional wheel–soil interaction model. In addition, it was difficult to implement these studies to the wheels of the rover. However, to introduce the online wheel performance estimation in a real mission, consideration of both wheel sinkage/slippage and reaction force/torque estimates is essential. Therefore, we have developed a sensing wheel system of wheel sinkage/slippage and reaction force/torque that can be implemented to each wheel of the rovers in future missions. Our previous work focused on estimating wheel sinkage/slippage online (Higa et al., 2016a). This paper reports reaction force/torque sensing using the wheel system that we developed.

## 2. Concept of a Sensing Wheel System for Wheel Performance Estimation

Figure 1 shows a conceptual diagram of the proposed system for wheel performance estimation. The system is composed of a wheel (driven by a rotary motor), a time-of-flight (ToF) camera, and a 6-axis force/torque (F/T) sensor. The ToF camera is used for online estimation of wheel sinkage and slippage. The ToF camera is a depth sensor and

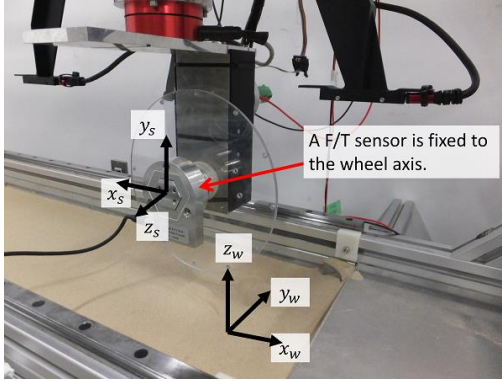


Fig. 2 F/T sensor fixed to the wheel axis.

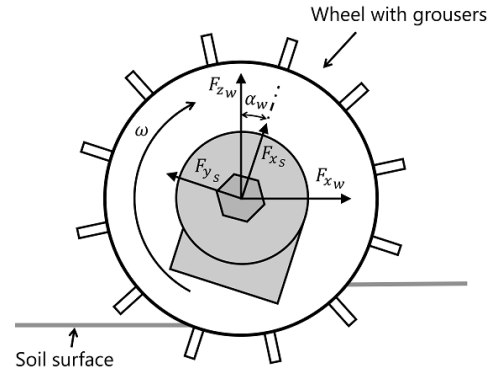


Fig. 3 F/T sensor fixed to the wheel axis.

outputs point cloud data of the depth from the sensor origin to the target object. The ToF camera can also capture 8-bit/16-bit monochrome images. Hence, wheel slippage estimation was performed based on the optical flow technique (Higa et al., 2016a). The wheel system can measure forces/torques in real time via a 6-axis F/T sensor. The test wheel is mounted on the wheel driving shaft via the F/T sensor. Thus, the F/T sensor can detect all reaction forces/torques that act from the traveling terrain. Accurate estimation of the wheel performance and terrain conditions can be provided by combining the F/T sensor data with the rover attitude data obtained from an internal measurement unit (IMU).

### 3. Real-Time Sensing of 6-axis Force/Torque of Proposed Wheel System

In order to maintain mobility control of lunar/planetary exploration rovers, the rover should be able to calculate the reaction forces/torques of the terrain it is traversing in real time. The stress measurement technique described earlier was accurate; however, it is not well suited to real-time operation, since several F/T sensors would be needed inside the wheel. Moreover, the update interval of the stress distribution is less than that required for mobility control, and the wheel maintains its traveling velocity during the stress measurements. Although accurate stress measurements are needed for effective estimates of wheel performance on loose soil and the target terrain/soil characteristics, the traveling control of the rover does not require the stresses distributed beneath the wheel, but rather requires the forces/torques acting on the wheel.

Therefore, in this section, we describe a real-time measurement method for the 6-axis force/torque acting on the center of a traveling wheel.

#### 3.1 Wheel configuration for real-time sensing of reaction forces/torques

To sense the 6-axis reaction forces/torques of the wheel on loose soil, we used a low-profile F/T sensor (FFS080F151M300R6; Leprino Co., Ltd.) shown in Fig. 2. The sensor can sense 3-axis forces up to  $\pm 150$  N and 3-axis torques up to  $\pm 30$  Nm.

The 6-axis F/T sensor was attached to the wheel shaft to measure the reaction forces/torques acting on the wheel in real time. The sensor rotates with the wheel, so the output fluctuates with the angle of wheel rotation. Thus, as shown in Fig. 3, the forces/torques acting on the wheel are projected as follows:

$$\begin{aligned}
 F_{xw} &= F_{xs} \sin \alpha_w - F_{ys} \cos \alpha_w, \\
 F_{yw} &= -F_{zs}, \\
 F_{zw} &= F_{xs} \cos \alpha_w - F_{ys} \sin \alpha_w, \\
 M_{xw} &= M_{xs} \sin \alpha_w - M_{ys} \cos \alpha_w, \\
 M_{yw} &= -M_{zs}, \\
 M_{zw} &= M_{xs} \sin \alpha_w - M_{ys} \cos \alpha_w,
 \end{aligned} \tag{1}$$

where the first index denotes the axis that each force or torque is acting on, the second index denotes the wheel coordinates or sensor coordinates, and  $\alpha_w$  is the angle of wheel rotation (counter-clockwise around the Y-axis of the wheel coordinates is positive).

The reaction forces/torques, which are projected by the above equations, require a precise angle of wheel rotation. In this system, the angle of wheel rotation is obtained from the wheel motor encoder at 50 Hz.

### 3.2 Calibration of real-time force/torque estimation

Single wheel tests were performed to validate the estimation of real-time force/torque acquisition. Before testing, the wheel sensor was calibrated. The calibration method was as follows:

1. Rotate the wheel several times in the air while obtaining sensor data.
2. Calculate the offset errors using the maximum and minimum values of each axis.
3. Subtract the offset errors in each axis.

## 4. Experimental Setup

Traction tests, using the single wheel testbed, were performed to confirm the proposed real-time force/torque sensing method. This section describes the single wheel testbed and experimental conditions.

### 4.1 Single wheel testbed

In this study, the single wheel testbed shown in Fig. 4 was used for evaluating the proposed sensing wheel system. The single wheel testbed, which includes the sandbox, is 2.50 m long, 1.05 m wide, and 1.45 m high. The testbed allows the test wheel to weigh up to 100 N and allows the wheel diameter of 250 mm to travel with a maximum sinkage of 85 mm on test soil. Furthermore, the wheel load can be adjusted by a load-canceling mechanism. Two types of experiments can be conducted using this testbed. One is a forced slip experiment in which a constant velocity is imposed on both the wheel motor and the conveying motor. The second is a traction load experiment in which the wheel motor maintains a constant velocity while pulling the wheel using several traction loads via pulleys and a rope. The traction load experiment was selected in this study.

The testbed consists of a wheel unit, a conveying unit, and a sandbox. The wheel unit consists of two vertical slide shafts with bushes, a wheel with a driving motor (speed-controlled by a microcontroller), a wheel load cancellation mechanism, and a linear encoder to count the wheel sinkage. The wheel can naturally sink into the soil in the vertical direction, along with the vertical slide shaft. The wheel is turned by a DC motor with a harmonic drive gear with a final gear ratio of 800:1. A microcontroller maintains a constant rotational velocity via a motor driver under proportional integral (PI) control at 10 ms intervals and measures the wheel sinkage by counting the linear encoder signals at the same intervals. The linear encoder resolution for the wheel sinkage measurement is 25  $\mu\text{m}$ . Measurements are calibrated by assigning a zero level to the soil surface.

The conveying unit consists of two linear guides to restrict motion in the horizontal direction, a conveying motor, and a linear encoder to count the wheel traveling distance measurement. The conveying motor and timing pulley are coupled, and the timing pulley is connected to the wheel unit via a timing belt. One of the two test conditions (forced constant-slip test or traction test using several traction loads) can be selected by connecting a rope to the timing belt. The linear encoder for the wheel traveling distance measurement is connected to the wheel unit. The conveying motor is also PI-controlled using a microcontroller via a motor driver at 10 ms intervals. The microcontroller counts the wheel traveling distance at the same intervals. The resolution of the linear encoder for the wheel traveling distance is 50  $\mu\text{m}$ .

The testbed is mounted on a sandbox with a length of 1.6 m, width of 0.3 m, and depth of 0.2 m. One of two isometric sandboxes can be selected to perform experiments, each using a different type of soil. One sandbox is filled with Toyoura sand, and the other is filled with lunar regolith simulant (FJS-1), manufactured by Shimizu Corporation. FJS-1 provides a good approximation for the soil characteristics on the moon's surface (Kanamori et al., 1998). Its grain size distribution is wider than that of Toyoura sand. The grain size of Toyoura sand is known to be nearly homogeneous, and its cohesion is almost exactly zero. In this study, we selected the Toyoura sand to validate the proposed system.

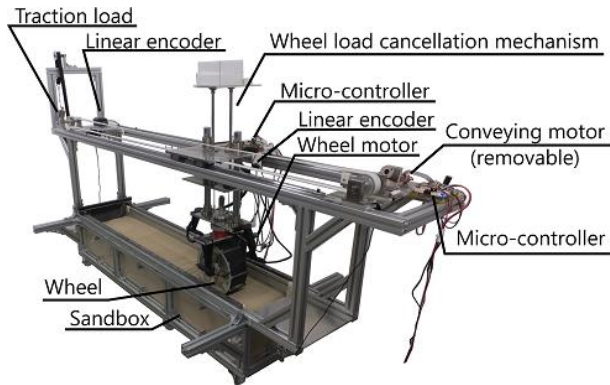


Fig. 4 Single wheel testbed.

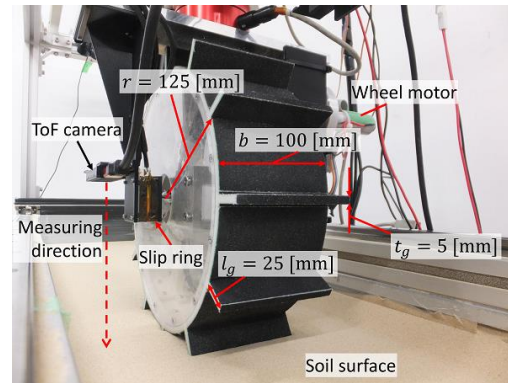


Fig. 5 A configuration of test wheel. (Grouser length is 25 mm.)

## 4.2 Experimental condition

Single-wheel tests under free slip conditions and with different traction loads ( $TL$ ) were performed using Toyoura sand as a test soil. The test wheel was  $\phi 250$  mm in diameter and 100 mm in width and weighed approximately 50 N. We tested the wheel with 25 mm grousers, 12.5 mm grousers, and no grousers. The angular velocity of the wheel was controlled to be 0.16 rad/s. Traction loads of 0, 10, and 20 N were applied to the wheels with grousers, and traction loads of 0, 5, and 10 N were applied to the smooth wheel. The slip ratio,  $s$ , of the test wheel is defined as follows:

$$s = \left( 1 - \frac{v_x}{(r + l_g)\omega} \right) \times 100, \quad (2)$$

where  $v_x$  is the traveling velocity of the wheel,  $r$  is the wheel radius,  $l_g$  is the length of the grousers, and  $\omega$  is the angular velocity of the wheel. The slip ratio is expressed as the ratio of the traveling speed of the wheel with grousers to the circumferential speed at the edge of a grouser; in general, the value of the slip ratio is between 0% and 100%. For instance, the case  $s = 0\%$  indicates that the rover can travel without slippage, and the case  $s = 100\%$  indicates that the wheel slips completely, and the rover cannot travel at all. The traveling velocity is counted by the horizontal linear encoder of the single wheel testbed. The angular velocity is acquired by the rotary encoder of the wheel motor.

## 5. Results and Discussions

Figures 6a, 7a, 8a, and 9a show the estimated drawbar pull, estimated normal force, estimated wheel torque, and angle of the resultant force of a wheel with no grousers, respectively. The median values of slip ratios under a steady state of the wheel with no grousers under traction loads of 0, 5, and 10 N were approximately 12.6%, 89.7%, and 95.5%, respectively. Figures 6b, 7b, 8b, and 9b show the estimated drawbar pull, estimated normal force, estimated wheel torque, and angle of the resultant force of a wheel with 12.5 mm grousers, respectively. The median values of slip ratios under a steady state of the wheel with 12.5 mm grousers under traction loads of 0, 10, and 20 N were approximately 15.2%, 59.6%, and 90.1%, respectively. Figures 6c, 7c, 8c, and 9c show the estimated drawbar pull, estimated normal force, estimated wheel torque, and angle of the resultant force of a wheel with 25 mm grousers, respectively. The median values of slip ratios under a steady state of the wheel with 25 mm grousers under traction loads of 0, 10, and 20 N were approximately 0%, 37.4%, and 79.9%, respectively.

### 5.1 Drawbar pull

As shown in Fig. 6, the estimated drawbar pull increases with the traction load. As wheel slippage is introduced via the traction load, each estimated drawbar pull converges under steady state conditions. If the experiments were performed under forced slip conditions, which forcibly maintain the constant traveling velocity of the wheel, the estimated drawbar pull would vary periodically because of the grousers (Ding et al., 2011). Although the estimated drawbar pull includes the viscosity resistance of the guide rail and the tension of the linear encoder, the difference in

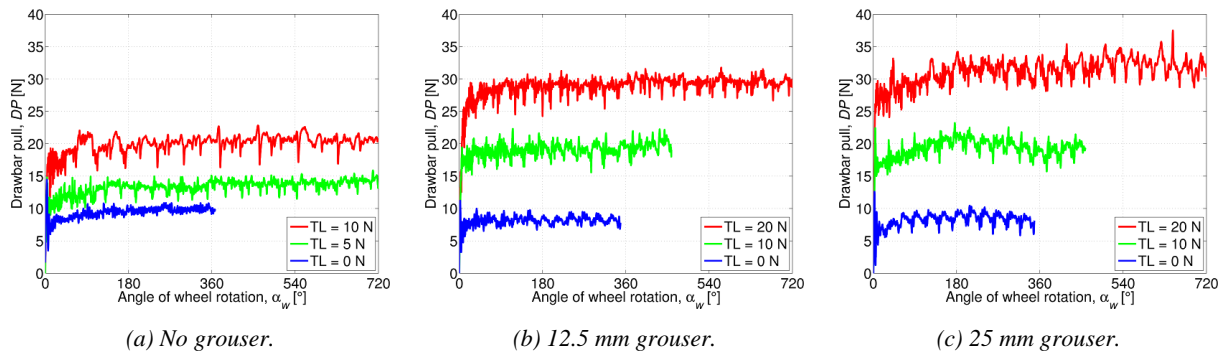


**Fig. 6** Drawbar pull estimated by the F/T sensor at wheel axle.

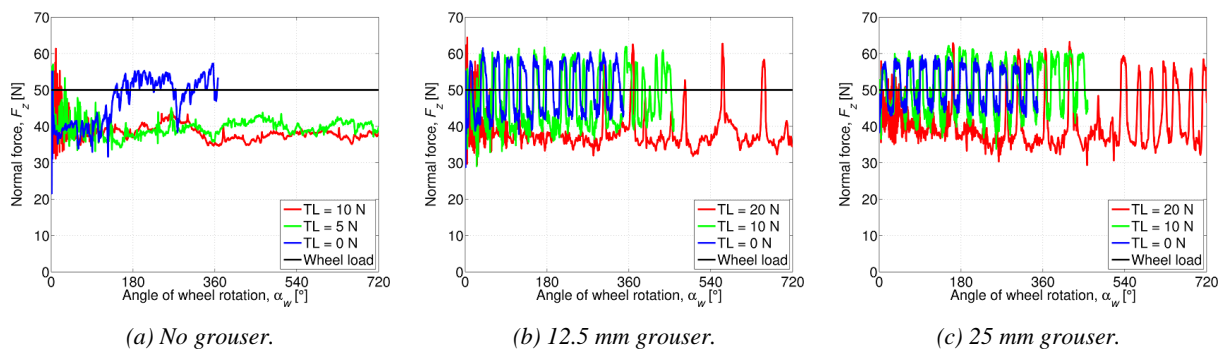


**Fig. 7** Normal force estimated by the F/T sensor at wheel axle.

each drawbar pull corresponds to the difference in traction load. Therefore, it can be concluded that the drawbar pull can be well estimated using the projection approach.

## 5.2 Normal force

As shown in Fig. 7, the estimated normal force fluctuates significantly. This phenomenon implies that each grouser interacts with the terrain beneath the test wheel. When the grousers exert additional tractive force, the normal force becomes larger than the wheel load. Thus, wheels with grousers are better than wheels without grousers. Moreover, although the traction loads are different, the maximum normal forces under each condition are similar. This phenomenon indicates that the maximum normal forces depend on the grouser length.

Adversely, the grousers induce soil failure by digging into the soil when they first make contact with the ground. This phenomenon is reflected in the estimated normal force. When the soil collapses under a grouser, it loses its bearing capacity. Thus, the normal force becomes less than the wheel load. This phenomenon becomes notable when the wheel slippage increases. The minimum normal forces under each traction load condition decrease as the traction load increases. Furthermore, when  $TL = 20$  N, most of the normal force is less than the wheel load until the angle of wheel rotation reaches  $540^\circ$ . After reaching  $540^\circ$ , the normal force periodically switches between its maximum and minimum. The wheel condition can be regarded as being in the steady state condition. This implies that the wheel condition can also be estimated from the normal force estimates.

## 5.3 Wheel torque

As shown in Fig. 8, the estimated wheel torque increases with the traction load. Moreover, the wheel torque fluctuates greatly, similar to the normal force. However, the amplitude of the wheel torque when  $TL = 20$  N decreases in comparison to the case for  $TL = 0$  N. This indicates that the wheel torque reaches a certain maximum and becomes saturated.

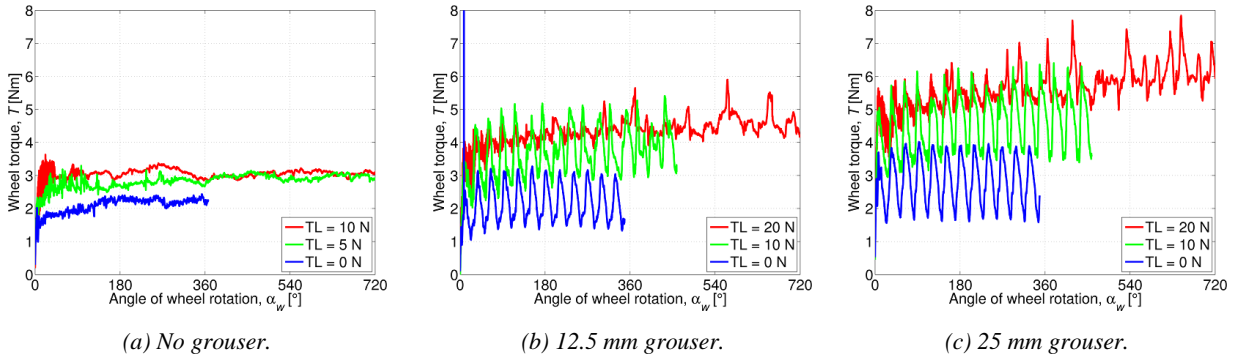


**Fig. 8** Wheel torque estimated by the F/T sensor at wheel axle.

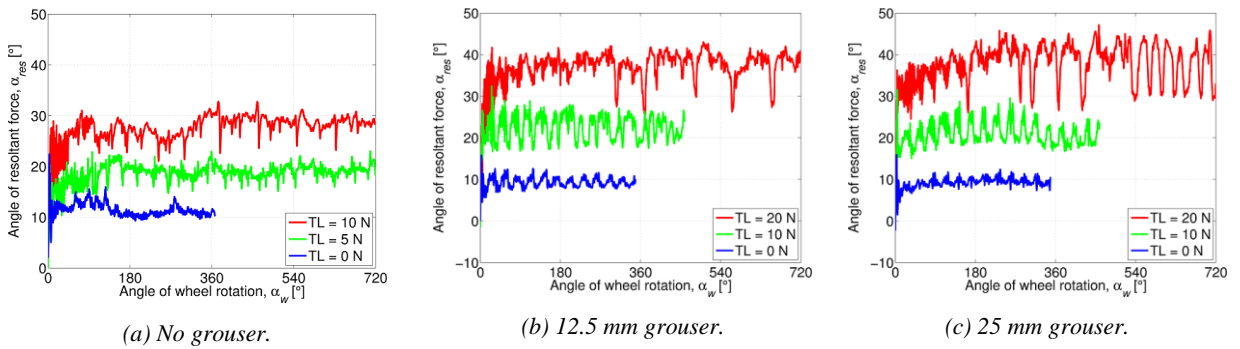


**Fig. 9** Angle of resultant force estimated by the F/T sensor at wheel axle.

It is known that wheel torque increases as the wheel sinks. Increasing the wheel sinkage widens the contact patch. Therefore, two or more grousers always exert traction. Thus, the amplitude of wheel torque under large traction loads is smaller than under low-traction conditions.

#### 5.4 Angle of resultant force

The angle of resultant force is proposed as an evaluation index. This is calculated from the ratio of drawbar pull to normal force as follows:

$$\alpha_{res} = \tan^{-1}\left(\frac{DP}{W}\right), \quad (3)$$

where  $DP$  and  $W$  denote the drawbar pull and normal force of a wheel, respectively.

As shown in Fig. 9, the estimated angle of resultant force increases with the traction load. Because the angle of the resultant force is calculated from the normal force, it fluctuates when the wheel has grousers. The estimated angles under each condition converge after the wheel reaches the steady state condition. The converged angle is close to the maximum stress angle of the stress distributions of a wheel without grousers under similar slip conditions. Although additional discussion regarding a relationship between the normal stress and the angle of resultant force is needed, the angle of resultant force may be used to estimate the maximum stress angle.

## 6. Conclusion

In this study, we proposed a real-time reaction force/torque sensing wheel system on loose soil for in situ monitoring. Real-time sensing of force/torque was realized by fixing a 6-axis F/T sensor to the wheel axle. The drawbar pull, normal force, and wheel torque were projected using the angle of wheel rotation. In particular, the drawbar pull and normal force revealed a correlation with wheel sinkage and slippage. This information is useful for traversal on

unknown loose terrain because the force information will detect whether the ground support is sufficient for the rover. Moreover, the angle of resultant force was also derived. Because this angle is calculated based on drawbar pull and normal force, the angle effectively indicates the direction of the dominant force. This implies that the angle of resultant force may support estimates of the maximum stress angle of a wheel.

## Nomenclature

$F_{xw}$	drawbar pull of a wheel	[N]
$F_{yw}$	side force of a wheel	[N]
$F_{zw}$	normal force of a wheel	[N]
$M_{xw}$	roll moment of a wheel	[Nm]
$M_{yw}$	pitch moment of a wheel (wheel torque)	[Nm]
$M_{zw}$	yaw moment of a wheel	[Nm]
$F_{xs}$	force in the x-axis of the F/T sensor coordinate	[N]
$F_{ys}$	force in the y-axis of the F/T sensor coordinate	[N]
$F_{zs}$	force in the z-axis of the F/T sensor coordinate	[N]
$M_{xs}$	moment in the x-axis of the F/T sensor coordinate	[Nm]
$M_{ys}$	moment in the y-axis of the F/T sensor coordinate	[Nm]
$M_{zs}$	moment in the z-axis of the F/T sensor coordinate	[Nm]
$\alpha_w$	angle of wheel rotation	[rad]
$s$	slip ratio	[%]
$v_x$	traveling velocity	[m/s]
$r$	wheel radius	[m]
$\omega$	angular velocity of the wheel	[rad/s]
$b$	wheel width	[m]
$l_g$	length of a grouser	[m]
$t_g$	thickness of a grouser	[m]
$TL$	traction load	[N]
$DP$	drawbar pull	[N]
$W$	normal force (wheel load)	[N]
$T$	wheel torque	[Nm]
$\alpha_{res}$	angle of the resultant force	[rad]

## Acknowledgements

This work was partially supported by JSPS KAKENHI, Grant-in-Aide for JSPS Research Fellow, Grant Number 16J02425.

## References

- Ding, L., Gao, H., Deng, Z., Nagatani, K., Yoshida, K., 2011. Experimental study and analysis on driving wheels' performance for planetary exploration rovers moving in deformable soil. *Journal of Terramechanics* 48, 27–45. doi:10.1016/j.jterra.2010.08.001
- Hegde, G.M., Ye, C., Robinson, C.A., Stroupe, A., Tunstel, E., 2013. Computer-vision-based wheel sinkage estimation for robot navigation on lunar terrain. *IEEE/ASME Transactions on Mechatronics* 18, 1346–1356. doi:10.1109/TMECH.2013.2264095
- Higa, S., Nagaoka, K., Yoshida, K., 2016a. Online estimation of wheel sinkage and slippage using a tof camera on loose soil, in: *Proceedings of the ISTVS 8th Americas Regional Conference*. Troy, MI, USA.

- Higa, S., Sawada, K., Nagaoka, K., Nagatani, K., Yoshida, K., 2016b. Measurement of stress distributions of a wheel with grousers traveling on loose soil, in: 2016 IEEE International Conference on Robotics and Automation (ICRA). IEEE, pp. 2828–2833. doi:10.1109/ICRA.2016.7487445
- Higa, S., Sawada, K., Nagaoka, K., Nagatani, K., Yoshida, K., 2015. Three-dimensional stress distribution on a rigid wheel surface for a lightweight vehicle, in: Proceedings of the 13th European Conference of the ISTVS. Rome, Italy, pp. 383–391.
- Iagnemma, K., Kang, S., Shibly, H., Dubowsky, S., 2004. Online Terrain Parameter Estimation for Wheeled Mobile Robots With Application to Planetary Rovers. *IEEE Transactions on Robotics* 20, 921–927. doi:10.1109/TRO.2004.829462
- Iizuka, K., Sasaki, T., Suzuki, S., Kawamura, T., Kubota, T., 2014a. Study on grouser mechanism to directly detect sinkage of wheel during traversing loose soil for lunar exploration rovers. *ROBOMECH Journal* 1, 15. doi:10.1186/s40648-014-0015-6
- Iizuka, K., Sasaki, T., Yamano, M., Kubota, T., 2014b. Development of Grousers with a Tactile Sensor for Wheels of Lunar Exploration Rovers to Measure Sinkage. *International Journal of Advanced Robotic Systems* 11, 49. doi:10.5772/57361
- Kanamori, H., Udagawa, S., Yoshida, T., Matsumoto, S., Takagi, K., 1998. Properties of Lunar Soil Simulant Manufactured in Japan. *Space 98 (6th)*, April 26-30 462–468. doi:10.1061/40339(206)53
- Milella, A., Reina, G., Siegwart, R., 2006. Computer Vision Methods for Improved Mobile Robot State Estimation in Challenging Terrains. *Journal of Multimedia* 1, 49–61. doi:10.4304/jmm.1.7.49-61
- Nagatani, K., Ikeda, A., Ishigami, G., Yoshida, K., Nagai, I., 2010. Development of a Visual Odometry System for a Wheeled Robot on Loose Soil using a Telecentric Camera. *Advanced Robotics* 24, 1149–1167. doi:10.1163/016918610X501282
- Nagatani, K., Ikeda, A., Sato, K., Yoshida, K., 2009. Accurate estimation of drawbar pull of wheeled mobile robots traversing sandy terrain using built-in force sensor array wheel, in: 2009 IEEE/RSJ International Conference on Intelligent Robots and Systems. IEEE, pp. 2373–2378. doi:10.1109/IROS.2009.5354566
- Ojeda, L., Cruz, D., Reina, G., Borenstein, J., 2006. Current-Based Slippage Detection and Odometry Correction for Mobile Robots and Planetary Rovers. *IEEE Transactions on Robotics* 22, 366–378. doi:10.1109/TRO.2005.862480
- Ray, L.E., 2009. Estimation of Terrain Forces and Parameters for Rigid-Wheeled Vehicles. *IEEE Transactions on Robotics* 25, 717–726. doi:10.1109/TRO.2009.2018971
- Reina, G., Ojeda, L., Milella, A., Borenstein, J., 2006. Wheel slippage and sinkage detection for planetary rovers. *IEEE/ASME Transactions on Mechatronics* 11, 185–195. doi:10.1109/TMECH.2006.871095
- Shirai, T., Ishigami, G., 2014. Accurate Estimation of Wheel Pressure-Sinkage Traits on Sandy Terrain using In-Wheel Sensor System, in: Proceedings of the 12th International Symposium on Artificial Intelligence, Robotics and Automation in Space (I-SAIRAS 2014). Session 8a-3.